Inorg. Chem. **2003**, *42*, 1448–1455

Photophysics and Redox Behavior of Chiral Transition Metal Polymers

Jason A. Barron, Samantha Glazier, Stefan Bernhard, Kazutake Takada, Paul L. Houston,* and Héctor D. Abruña*

Department of Chemistry and Chemical Biology, Baker Laboratory, Cornell University, Ithaca, New York 14853-1301

Received November 1, 2002

The absorption and emission spectra, excited-state lifetimes, quantum yields, and electrochemical measurements have been obtained for a new series of chiral complexes based on three different chiral 2,2′:6′,2′′-terpyridine ligands, (–)-ctpy, (–)-[ctpy-x-ctpy], and (–)-[ctpy-b-ctpy], with one, two, or multiple Ru metal centers. The room-temperature absorption and emission maxima of {[((–)-ctpy)Ru]-(–)-[ctpy-b-ctpy]-[Ru((–)-ctpy)]}$(PF_6)_4$ and ((–)-[ctpy-b-ctpy])-{[Ru((–)-[ctpy-b-ctpy])]$(PF_6)_2$}$_n$ were shifted to lower energies and also exhibited significantly longer luminescence lifetimes when compared to [Ru((–)-ctpy)$_2$]$(PF_6)_2$, {[((–)-ctpy)Ru]-(–)-[ctpy-x-ctpy]-[Ru((–)-ctpy)]}-$(PF_6)_4$, and ((–)-[ctpy-x-ctpy])-{[Ru((–)-[ctpy-x-ctpy])]$(PF_6)_2$}$_n$. In terms of their electrochemical behavior, all of the complexes studied exhibited one Ru-centered and two ligand-centered redox waves and the {[((–)-ctpy)Ru]-(–)-[ctpy-x-ctpy]-[Ru((–)-ctpy)]}$(PF_6)_4$, ((–)-[ctpy-x-ctpy])-{[Ru((–)-[ctpy-x-ctpy])]$(PF_6)_2$}$_n$, and ((–)-[ctpy-b-ctpy])-{[Ru-((–)-[ctpy-b-ctpy])]$(PF_6)_2$}$_n$ complexes were found to electrodeposit upon ligand-based reduction. The difference between the formal potentials of the Ru-centered and the first ligand-centered (least negative) waves corresponded linearly with the changes in the observed emission energies. The shifts in energy are discussed using a particle-in-a-box model, and the luminescence lifetimes are discussed in terms of the structure of the excited-state manifold.

Introduction

Chirality and stereochemistry are subjects of broad interest and profound importance in chemistry and biology. In these areas, the effects of chirality and stereochemistry have been, and continue to be, intensely investigated. The study of chirality in transition metal systems is one that has not been traditionally explored but which has seen a great deal of growth in recent times, in part, due to their potential applications as nonlinear optical materials and as electrocatalysts for enantioselective transformations.[1−4] The use of nonlinear materials in the liquid phase would be attractive because they would be less susceptible to damage than crystals.[5] While the strength of the nonlinear response from the materials in the liquid phase studied to date has been weak,[6−9] developing new nonlinear solid materials has been limited by the need to produce homogeneous crystals. Further, the complexation of multiple chiral organometallic systems into a polymer would provide for the possibility of generating nonlinear photosensitive macromolecular species.

We report on the synthesis and characterization of a novel series of chiral ruthenium-containing terpyridyl-based compounds. These compounds, presented in Figure 1, were synthesized from modified, enantomerically pure terpyridyl ligands to yield chiral final products. On the basis of these materials, we have been able to prepare mono-, di-, and polynuclear transition metal complexes of Ru. Because of the extraordinary complexity involved in using IUPAC names, we have employed a more trivial naming system. Ligand **X** in Figure 1 is referred to as (−)-[ctpy-x-ctpy], and

* To whom correspondence should be addressed. E-mail: hda1@cornell.edu (H.D.A.).

(1) Long, N. J. *Angew. Chem., Int. Ed. Engl.* **1995**, *34*, 21.
(2) Marder, S. R. In *Inorganic Materials*; Bruce, D. W., O'Hare, D., Eds.; John Wiley & Sons: New York, 1992; pp 115−164.
(3) Whittall, I. R.; McDonagh, A. M.; Humphrey, M. G.; Samoc, M. *Adv. Organometallic Chem.* **1998**, *42*, 291−362.
(4) Whittall, I. R.; McDonagh, A. M.; Humphrey, M. G.; Samoc, M. *Adv. Organometallic Chem.* **1998**, *43*, 349−405.
(5) Fischer, P.; Wiersma, D. S.; Righini, R.; Champagne, B.; Buckigham, A. D. *Phys. Rev. Lett.* **2000**, *85*, 4253−4256.
(6) McDonagh, A. M.; Humphrey, M. G.; Samoc, M.; Luther-Davies, B.; Houbrechts, S.; Wada, T.; Sasabe, H.; Persoons, A. *J. Am. Chem. Soc.* **1999**, *121*, 1405−1406.
(7) Mesnil, H.; Hache, F. *Phys. Rev. Lett.* **2000**, *85*, 4257−4260.
(8) Fischer, P.; Wiersma, D. S.; Righini, R.; Champagne, B.; Buckingham, D. A. *Phys. Rev. Lett.* **2000**, *85*, 4253−4256.
(9) Belkin, M. A.; Kulakov, T. A.; Ernst, K.-H.; Yan, L.; Shen, Y. R. *Phys. Rev. Lett.* **2000**, *85*, 4474−4477.

10.1021/ic020691v CCC: $25.00
Published on Web 02/04/2003

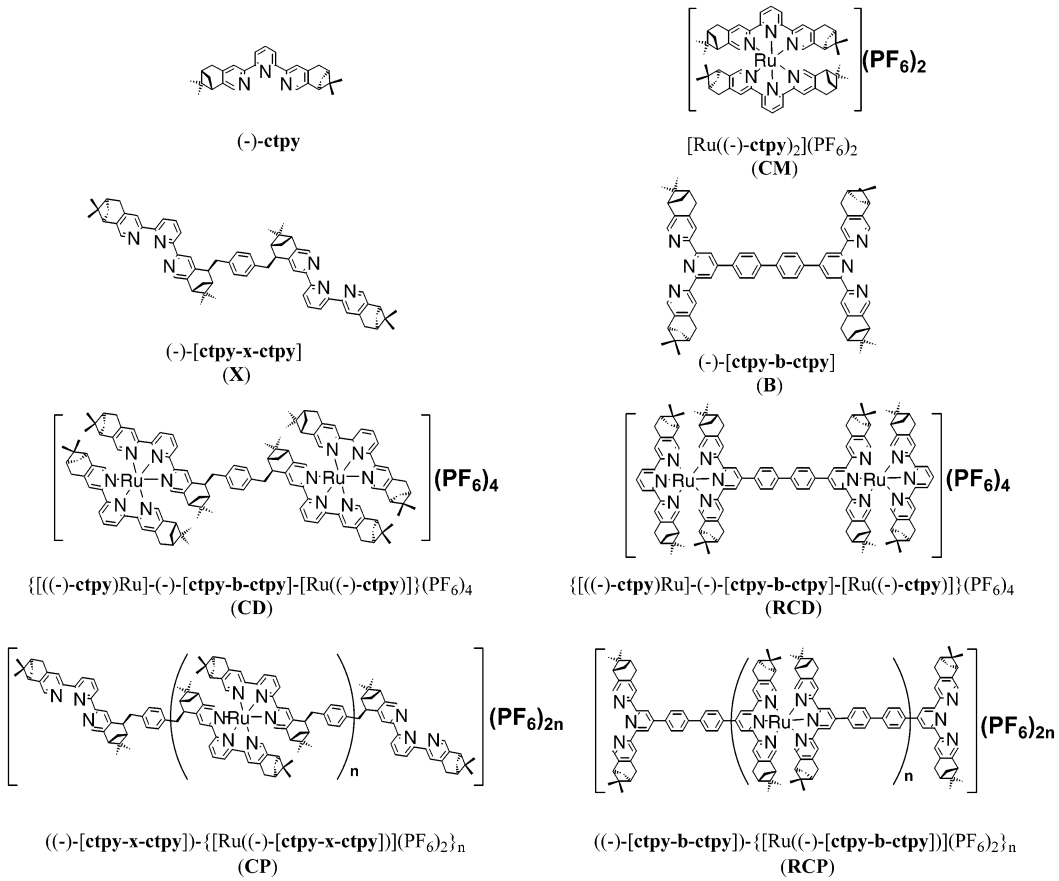

Figure 1. Schematic representation of the 2,2′:6′,2″-terpyridine complexes of ruthenium **CM**, **CD**, **CP**, **RCD**, and **RCP** and the corresponding ligands [ctpy-x-ctpy] and [ctpy-b-ctpy].

the dimer and polymer materials derived from it are referred to as "chiral dimer" and "chiral polymer", respectively. In addition, and for comparison, we have also prepared a monomeric complex using the chiral terpyridine ligand (−)-ctpy and we refer to this complex as "chiral monomer". The sterically more rigid ligand **B** in Figure 1 is referred to as (−)-[ctpy-b-ctpy], and we have prepared the corresponding dimer and polymer as well.

In recent work, we have reported on the synthesis and characterization of analogous complexes of Fe where we could unambiguously establish the chirality of the redox polymers via CD spectroscopy.[10] We have also recently presented work on the photochemistry and photophysics of PAMAM dendrimers with pendant $[Ru(bpy)_3]^{2+}$ and $[Ru(tpy)_2]^{2+}$ chromophores.[11] In that work we studied the rather complex relationship between the chromophore and its surrounding environment. In this article we present the synthesis and investigate the photophysical and electrochemical behavior of chiral photo- and redox-active transition metal complex monomers, dimers, and polymers.

Experimental Section

Synthesis. The synthesis of the ligands and metal complexes was carried out as recently described.[10] The ligands and metal complexes employed are presented in Figure 1. A Varian Inova-400 spectrometer was used to collect ^{1}H and ^{13}C NMR data. The precursor Ru((−)-ctpy)Cl_3 was prepared as previously described in the literature.[12] To simplify identification of the metal complexes, the following abbreviations were employed:

(1) $[Ru((-)\text{-ctpy})_2](PF_6)_2$ = chiral monomer (**CM**);

(2) $\{[((-)\text{-ctpy})Ru]\text{-}(-)\text{-}[ctpy\text{-}b\text{-}ctpy]\text{-}[Ru((-)\text{-ctpy})]\}(PF_6)_4$ = chiral dimer (**CD**);

(3) $((-)\text{-}[ctpy\text{-}x\text{-}ctpy])\text{-}\{[Ru((-)\text{-}[ctpy\text{-}x\text{-}ctpy])](PF_6)_2\}_n$ = chiral polymer (**CP**);

(4) $\{[((-)\text{-ctpy})Ru]\text{-}(-)\text{-}[ctpy\text{-}b\text{-}ctpy]\text{-}[Ru((-)\text{-ctpy})]\}(PF_6)_4$ = rigid chiral dimer (**RCD**);

(5) $((-)\text{-}[ctpy\text{-}b\text{-}ctpy])\text{-}\{[Ru((-)\text{-}[ctpy\text{-}b\text{-}ctpy])](PF_6)_2\}_n$ = rigid chiral polymer (**RCP**).

[Ru((−)-ctpy)$_2$](PF$_6$)$_2$ (CM). A 22.2 mg amount of $RuCl_3$ hydrate (107 mmol) and 100 mg of (−)-ctpy (0.237 mmol) were suspended in 10 mL of ethane-1,2-diol, and the mixture was refluxed in a microwave oven for 8 min. The solution immediately turned orange. A 50 mL volume of water was added after the solution cooled to room temperature, and the resulting solution was filtered through Celite. A solution of 1 g of NH_4PF_6 in water was added to the filtrate, and the resulting precipitate was filtered off. The complex was purified by recrystallization from acetone/ether. Yield: 114 mg (86%).

^{1}H NMR (acetone-d_6, 400 MHz): δ 8.87 (2H, d, $J^3(H^{3'}H^{4'})$ = 16.1, H(3′, 5′)), 8.56 (2H, s, H(3, 3″)), 8.43 (1H, dd, $J^3(H^{4'}H^{3'})$ = 12.0, $J^3(H^{4'}H^{5'})$ = 12.0, H(4′)), 7.18 (2H, s, H(6, 6″)), 3.19 (4H,

(10) Bernhard, S.; Takada, K.; Díaz, D. J.; Abruña, H. D.; Mürner, H. *J. Am. Chem. Soc.* **2001**, *123*, 10, 265−210, 271.

(11) Glazier, S.; Barron, J.; Houston, P. L.; Abruña, H. D. *J. Phys. Chem. B* **2002**, *106*, 9993−10003.

(12) Sullivan, B. P.; Calvert, J. M.; Meyer, T. J. *Inorg. Chem.* **1980**, *19*, 1404−1407.

m, H(7)), 2.60−2.44 (4H, m, H(10, 10″, 11b, 11b″)), 2.20 (m, 2H, H(8, 8")), 1.18 (6H, s, H(12, 12″)), 0.89 (2H, d, $J^3(H^{11a}H^{11b}) = 11.0$, H(11a, 11a″), 0.15 (6H, s, H(13, 13″)).

MS (ESI) *m*/*z* 472.6 (100%, $[M - 2PF_6]^{2+}$). HR-MS (ESI): calcd for $C_{58}H_{62}N_6Ru$ ($[M - 2PF_6]^{2+}$), 472.203 97; found, 472.203 89.

Optical absorption [ϵ(480 nm)]: 4100 M^{-1} cm^{-1}.

{[((−)-ctpy)Ru]-(−)-[ctpy-x-ctpy]-[Ru((−)-ctpy)]}$(PF_6)_4$ (CD). A 25 mg amount of Ru((−)-ctpy)Cl_3 (0.04 mmol) and 20 mg of (−)-[ctpy-x-ctpy] (0.021 mmol) in 10 mL of ethane-1,2-diol were refluxed in a microwave oven. The orange solution was allowed to cool to room temperature and was added to 50 mL of water. After the solution was filtered through Celite, a solution of 1 g of NH_4PF_6 in water was added and the formed precipitate was filtered off. The complex was purified by column chromatography on aluminum oxide with acetone and an increasing amount of water as eluent. Yield: 37 mg (68%).

^{1}H NMR (acetone-d_6, 400 MHz): δ 8.90 (1H, d, $J = 16$), 8.87 (2H, d, $J = 17$), 8.84 (1H, d, $J = 16$), 8.56 (3H, s), 8.54 (1H, s), 8.43 (1H, dd, $J_1 = 12.0$, $J_2 = 12.0$), 8.42 (1H, dd, $J_1 = 12.0$, $J_2 = 12.0$), 7.25 (1H, s), 7.24 (1H, s), 7.21 (1H, d, $J = 9.7$), 7.22 (2H, s), 7.16 (1H, d, $J = 9.7$), 3.6−3.3 (2H, m, H(CH_2, xylyl)), 3.25−3.05 (7H, m), 3.0−2.8 (4H, m), 2.50 (4H, bs), 2.41 (1H, bs), 2.21 (2H, bs), 1.95 (1H, bs), 1.60−1.42 (1H, m), 1.19 (9H, s, H(CH_3: (−)-ctpy, (−)-[ctpy-b-ctpy])), 1.11 (3H, s, H(CH_3: (−)-[ctpy-b-ctpy])), 0.94 (3H, bt), 0.23 (6H, s, H(CH_3: (−)-ctpy)), 0.22 (3H, s, H(CH_3: (−)-[ctpy-b-ctpy])), 0.16 (3H, s, H(CH_3: (−)-[ctpy-b-ctpy])).

MS (ESI) *m*/*e* 497.7 (100%, $[M - 4PF_6]^{4+}$). HR-MS (ESI): calcd for $C_{124}H_{130}N_{12}Ru_2$ ($[M - 4PF_6]^{4+}$), 497.717; found, 497.709.

Optical absorption [ϵ(481 nm)]: 9400 M^{-1} cm^{-1}.

{[((−)-ctpy)Ru]-(−)-[ctpy-b-ctpy]-[Ru((−)-ctpy)]}$(PF_6)_4$ (RCD). A synthetic procedure identical to the one described above for {[((−)-ctpy)Ru]-(−)-[ctpy-b-ctpy]-[Ru((−)-ctpy)]}$(PF_6)_4$ was used to prepare this dinuclear complex. Yield: 25 mg (48%).

^{1}H NMR (acetone-d_6, 400 MHz): δ 9.37 (2H, s), 8.92 (2H, d, $J = 8.1$), 8.86 (2H, s), 8.60 (2H, s), 8.56 (2H, d, $J = 8.3$), 8.48 (1H, t, $J = 8.3$), 8.23 (2H, d, $J = 8.3$), 7.33 (2H, s), 7.23 (2H, s), 3.28−3.10 (8H, m), 2.60−2.49 (8H, m), 2.24 (4H, bs), 1.21 (3H, s), 1.20 (3H, s), 1.17 (6H, s), 0.99 (2H, d, $J = 9.8$), 0.97 (2H, d, $J = 9.3$), 0.27 (9H, bs).

MS (ESI): *m*/*e* 510 (100%, $[M - 4PF_6]^{4+}$), 727.6 (100%, $[M - 3PF_6]^{3+}$).

Optical absorption [ϵ(493 nm)]: 18 500 M^{-1} cm^{-1}.

((−)-[ctpy-x-ctpy])-{[Ru((−)-[ctpy-x-ctpy])]$(PF_6)_2$}$_n$ (CP). A 20 mg amount of (−)-[ctpy-x-ctpy] (0.021 mmol) and 10.2 mg of $Ru(DMSO)_4Cl_2$ (0.02 mmol) were dissolved in 10 mL of absolute ethanol, and the resulting solution was refluxed for 24 h. After the solution was cooled to room temperature, 50 mL of water were added and the solution was extracted with 3 × 50 mL of hexane. The polymer was precipitated from the aqueous phase through the addition of 1 g of NH_4PF_6 in 5 mL of water. The dark orange crystals were collected through vacuum filtration. The complex was purified by recrystallization from acetone/ether. Yield: 21 mg (75%).

^{1}H NMR (acetone-d_6, 400 MHz): δ 9.0−8.8 (2H, m), 9.55 (2H, bs), 9.4−9.5 (1H, m), 7.40−7.05 (2H, m), 3.64−3.25 (2H, m), 3.18 (3H, bs), 2.72 (1H, bs), 2.31−2.60 (3H, m), 2.21 (1H, bs), 1.92 (1H, bs), 1.50−1.38 (1H, m), 1.23 (3H, s) 1.19 (3H, s), 1.07−0.97 (1H, m), 0.26 (3H, s), 0.19 (3H, s).

Optical absorption [ϵ(481 nm)]: 9400 M^{-1} cm^{-1}.

((−)-[ctpy-b-ctpy])-{[Ru((−)-[ctpy-b-ctpy])]$(PF_6)_2$}$_n$ (RCP). A synthetic procedure identical to the one described above for ((−)-[ctpy-x-ctpy])-{[Ru((−)-[ctpy-x-ctpy])]$(PF_6)_2$}$_n$ was used to prepare this polymeric complex.

Yield: 18 mg (62%).

^{1}H NMR (acetone-d_6, 400 MHz): δ 9.35 (1H, bs), 8.86 (1H, bs), 8.74−8.04 (2H, m), 7.35 (1H, bs), 3.20 (2H, bq), 2.52 (2H, bs), 2.25 (1H, bs), 1.21 (3H, bs), 1.01 (1H, bs), 0.30 (3H, bs).

Optical absorption [ϵ(503 nm)]: 32 900 M^{-1} cm^{-1}.

Materials and Solvents. Acetonitrile was purchased from Burdick and Jackson and dried over 4 Å molecular sieves. Butyronitrile was purchased from Aldrich (98%), distilled, and dried over 4 Å molecular sieves. Tetra-*n*-butylammonium hexafluorophosphate (TBAH; G. F. Smith) was recrystallized three times from ethyl acetate and dried under vacuum for 72 h. All glassware was cleaned in a chromerge bath and rinsed in Millipore ultrapure water with a resistivity greater than 18 MΩ. Fluorescence cuvettes were cleaned with "piranha" solution (4:1 concentrated sulfuric acid 30% hydrogen peroxide). Samples for room-temperature measurements were prepared in quartz fluorescence cuvettes or NMR tubes (Kontes Glass) and degassed for more than 20 min with N_2 before measurement. Low-temperature glasses were found to form best when a distilled butyronitrile solution was employed. This allowed for a stable glass that was fairly resistant to cracking even under irradiation with peak laser powers greater than 5 kW. Samples were prepared in NMR tubes and placed in a clear glass dewar containing liquid nitrogen. Samples used in luminescence emission experiments had concentrations of 6.0 μM (**CM**), 1.3 μM (**CD**), 4.0 μM (**CP**), 3.8 μM (**RCD**), and 3.5 μM (**RCP**).

Apparatus. Room-temperature experiments were carried out using a time-correlated single photon counting apparatus (TCSPC). It consisted of a mode-locked Spectra Physics Tsunami Ti:saphire laser (82 MHz rep rate) which was pumped by a Spectra Physics Argon ion laser (13 W). Pulses were less than 100 fs fwhm. The bandwidth was monitored via an Ist-rees laser spectral analyzer during the experiment. Laser light was doubled in a BBO (β-barium borate) crystal to provide excitation wavelengths from 380 to 420 nm. The power was approximately 20 mW. The beam was filtered and focused onto a 1 cm^2 fluorescence cell, and the output was collected at 90°. The fluorescence was collimated with a 2 in. collection lens (2 in. focal length), filtered, and focused onto a single monochromator (2.5 mm slits). The signal was collected with a Hamamatsu PMT-MCP (R1564-07) cooled to −20 °C. It was then amplified using an EG&G Ortec 9306 1-GHz preamp and fed into a Becker and Hickl SPC-300 computer module. The start pulse was obtained by focusing a reflection of the fundamental beam onto a Becker and Hickl PHD-400-N photodiode. The start pulses were monitored with a Lecroy digital oscilloscope. Time-correlated single-photon counting was accomplished with a Becker and Hickl GmbH SPC-300 TCSPC module. This module contained the constant fraction discriminator, analog-to-digital converter, and time-to-amplitude converter. It used a reversed start−stop system to provide 13 ps time resolution and repetition rates of 200 MHz.

Low-temperature experiments were carried out using a Quanta Ray DCR Nd:YAG, frequency tripled to provide 150 mJ at 193 nm and 10 Hz, which, in turn, pumped a Lambda Physik dye laser using Coumarin 450 laser dye to provide 500 μJ of light at 460 nm. Pulses were 10 ns fwhm. Clear stable glasses were formed from samples cooled in glass NMR tubes placed in a glass dewar filled with liquid nitrogen. Fluorescence was collected at 90 degrees. A 2 in. collection lens was used in conjunction with a focusing lens and several filters (OG570, RG590, RG610) to bring the fluorescence onto a single monochromator (Bausch & Lomb) equipped with a PMT (Hamamatsu E990-07). Data were collected on a Lecroy digital oscilloscope, converted into ASCII format, and analyzed with Origin 6.1 computer software.

Data Analysis. Room-temperature data were deconvoluted and fit through the use of the SPCFit program provided by Dr. Ahmed Heikel. This program allowed for first-, second-, or third-order exponential fitting as well as deconvolution of the laser pulse width. Low-temperature data were fit using Origin 6.1.

Spectrofluorometer. Fluorescence spectra were obtained using a SPEX 1681 Minimate-2 spectrofluorometer with a Spectra Acq CPU controller. Low-temperature samples were measured in NMR tubes using butyronitrile as the solvent. All spectra were acquired at 90° to the incident radiation.

Quantum yield measurements were made using the SPEX 1681 Minimate-2 spectrofluorometer. All samples were measured under the same conditions to provide relative quantum yields compared to $[Ru(bpy)_3]^{2+}$ and $[Ru(tpy)_2]^{2+}$ standard solutions (10 μM). Quantum yield values for these materials were obtained from ref 21. As in the case of fluorescence measurements, low-temperature quantum yield measurements were done in NMR tubes in a quartz dewar. Measurements were done at least three times and averaged to correct for any errors due to small variations in sample placement. All measurements were found to be within 5% of the mean.

UV−Vis. UV−visible data were obtained using a HP-8453 diode array spectrometer. Sample spectra were obtained in quartz cuvettes (room temperature) or NMR tubes (low temperature). Absorbance maxima were kept below 0.5 to stay within the linear region of the Beer−Lambert law in calculating the molar absorptivities for the compounds. In calculating molar absorptivity values, we employed the weight of the sample and assumed a molecular weight corresponding to a single molecule (repeat unit in the polymer). There is a slight error in this as it does not account for the "end groups". However, given the relative masses involved, we believe the error to be minimal.

Electrochemical Measurements. Electrochemical experiments were carried out with a BAS CV-27 potentiostat. Three-compartment electrochemical cells (separated by medium-porosity sintered glass disks) with the provision for gas addition were employed. All joints were standard taper so that all compartments could be hermetically sealed with Teflon adapters. A platinum disk (geometric area = 0.008 cm^2) was used as a working electrode. The electrode was polished prior to use with 1 μm diamond paste (Buehler) and rinsed thoroughly with water and acetone. A large area platinum wire coil was used as a counter electrode. All potentials are referenced to a saturated Ag/AgCl electrode without regard for the liquid junction potential.

Results

Synthesis. The preparation of the mono- and dinuclear ruthenium complexes (**CM**, **CD**, **RCD**) was performed by employing traditional methods starting from $RuCl_3$ or Ru((−)-ctpy)Cl_3. For the synthesis of the polymeric complexes (**CP**, **RCP**) it was necessary to employ the Ru(II) precursor ($Ru(DMSO)_4Cl_2$). Moreover, the vigorous conditions during microwave irradiation in ethylene glycol lead to unsatisfactory purity of the isolated polymers; however, heating in ethanol yielded polymers of higher purity. It needs to be mentioned that for the following studies the pinene moieties attached to the bridging ligands serve only the purpose of enabling the solubilization of the chiral polymers. Studies describing the stereochemistry and the chiroptical properties of these new materials will be presented elsewhere.

Moreover, we have previously described the synthesis and characterization of analogous iron complexes where we were able to unambiguously establish the chiral nature of these materials through the use of circular dichroism and STM (see ref 10).

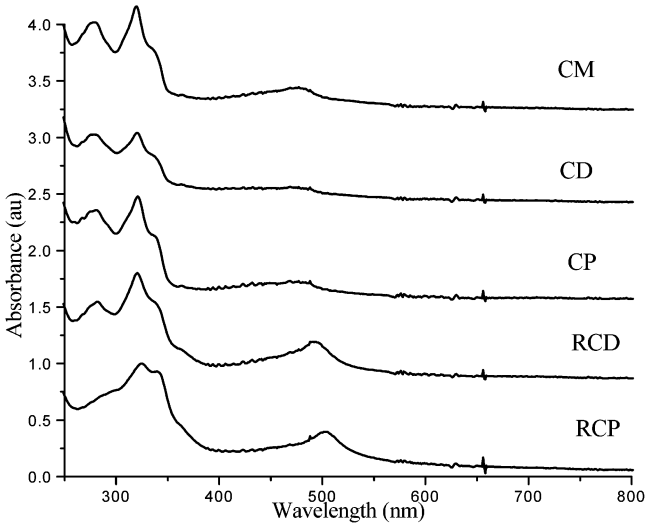

Figure 2. UV−vis absorption spectra for all compounds at 298 K in butyronitrile.

In addition, a word concerning the polymeric nature of materials such as **CP** and **RCP** is warranted. As we have reported on previously,[10] it is difficult to establish the degree of polymerization of these materials. In our previous study, we employed elemental analysis, gel permeation chromatography, vapor phase osmometry, STM, and electrospray ionization mass spectrometry in an attempt to estimate the degree of polymerization. However, each of the above techniques has its limitations. Nevertheless, from a combination of these techniques, we could establish that we are likely dealing with oligomers whose size is between 40 and 60 units. Trying to make a more precise estimate would be, in our view, speculative.

UV−Vis. The ultraviolet−visible spectra of all compounds studied are shown in Figure 2 and were similar to that of the $[Ru(tpy)_2]^{2+}$ reference compound. The band maxima are reported in Table 1. All compounds showed strong ligand-centered (LC) bands around 320 nm with a shoulder near 335 nm; both of these transitions were red shifted with respect to $[Ru(tpy)_2]^{2+}$ as expected due to the modification of the terpyridyl group. The LC shoulder of the CP was centered at 338. As anticipated, the chiral series (**CM**, **CD**, **CP**) exhibited an intense metal-to-ligand charge transfer (MLCT) band centered at 475 nm.

In the case of the rigid chiral series (**RCD**, **RCP**), we observed somewhat different trends. The LC shoulder was slightly red shifted for the **RCD** and **RCP** with respect to the **CM** by 3 and 6 nm, respectively. Further, the shoulder observed in both the chiral series and in the **RCD** was resolved as a second peak for the **RCP**. The MLCT bands for the **RCD** and the **RCP** showed significant red shifts to 492 and 503 nm, respectively, consistent with the higher conjugation present in these materials. It is also worth noting the significantly higher molar absorptivity of the **RCP** when compared to the **CP**. We believe that the increased rigidity of **RCP** vs **CP** makes the system more delocalized (as

Table 1. Summary of Photophysical Data for All Compounds at 77 K (10% Ethanol−90% Butyronitrile Mixture) and 298 K (Butyronitirile)

	abs (nm)		emission (nm)		t		f	
	LC	MLCT	298 K	77 K	298 K (ns)	77 K (μs)	298 K	77 K
$[Ru(tpy)_2]^{2+}$	310 (327)	477	615	603.5	125	11.1	(10×10^{-7})	(0.48)
CM	320 (335)	475	613	600.0	280	14.0	4×10^{-7}	0.18
CD	321 (335)	475	615	604.5	345	12.6	2×10^{-7}	0.11
CP	322 (338)	475	618	606.0	365	10.2	3×10^{-7}	0.13
RCD	321 (338)	492	(615)	633.0	3300	11.6	2×10^{-7}	0.08
RCP	325 (341)	503	(615)	637.5	1100	10.8	2×10^{-7}	0.09

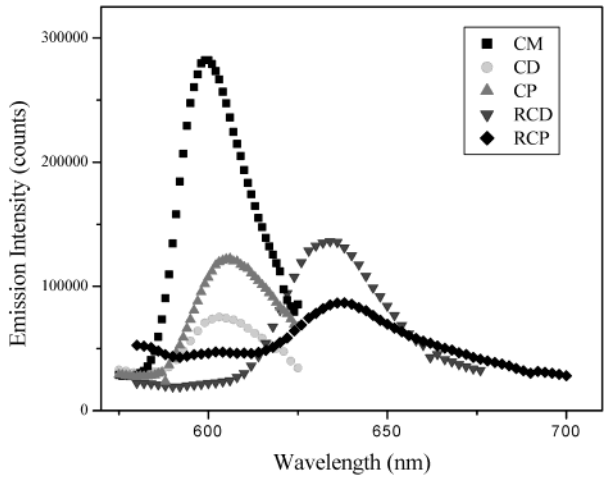

Figure 3. Emission decay spectra for all compounds at 77 K in a 10% ethanol−90% butyronitrile mixture.

mentioned above) giving rise to two effects, a red-shift in the absorption as alluded to above and an increase in the molar absorptivity. Whereas the general direction of the changes would be anticipated, the difference in magnitude especially for the molar absorptivity was not.

Emission Spectra. The low-temperature (77 K) emission spectra of **CM**, **CD**, **CP**, **RCD**, and **RCP** are shown in Figure 3. The emission maxima are given in Table 1 for the chiral series and $[Ru(tpy)_2]^{2+}$ used as a reference. As anticipated, the nonrigid chiral series had emission wavelengths similar to those of $[Ru(tpy)_2]^{2+}$. However, there were noticeable shifts in the emission peak. In the case of the **CM**, the emission maximum was blue shifted by 83 cm^{-1} to 600.0 nm (16 670 cm^{-1}). The **CD** was red shifted with respect to both $[Ru(tpy)_2]^{2+}$ and the **CM** with an emission peak at 604.5 nm (16 540 cm^{-1}). The **CP** emission peak was centered at 606.0 nm (16 500 cm^{-1}).

The rigid chiral series showed a significant red shift in emission wavelength to 633 nm (15 800 cm^{-1}) for the dimer (**RCD**) and 637.5 nm (15 690 cm^{-1}) for the polymer. These represent drops of 125 cm^{-1} for the dimer and 165 cm^{-1} for the polymer (**RCP**) relative to $[Ru(tpy)_2]^{2+}$.

Due to the very low quantum yields of these compounds, it was not possible to obtain well-resolved emission spectra at room temperature. The emission for all compounds was centered around 615.0 nm, a value similar to that of the reference compound, $[Ru(tpy)_2]^{2+}$.

Luminescence Quantum Yield at 77 K. Low-temperature quantum yields were determined by using the total counts from the principal emission peaks and comparing the value to the emission for $[Ru(tpy)_2]^{2+}$ under the same conditions. The values given in the table are not normalized to the number of ruthenium centers since the number for the polymers is not know precisely. Whereas the quantum yield for the **CM** was 0.18, which is about 1/3 that of $[Ru(tpy)_2]^{2+}$, the **CD** and **CP** had quantum yields of 0.11 and 0.13, respectively. The rigid chiral series exhibited slightly lower quantum yields with values of 0.08 for the **RCD** and 0.09 for the **RCP**.

The quantum yield values at 77 K were used to calculate the nonradiative and radiative rates at 77 K. Since the RT (room temperature) emission intensity was very weak, we used the relative values obtained at LT (low temperature) to estimate the quantum yields at room temperature.

Luminescence Lifetimes at 77 K. Low-temperature luminescence lifetimes for the chiral series were obtained at 77 K in butyronitrile. The lifetimes calculated from fitting the data to a single-exponential decay (Table 1) were 14.0 μs for the **CM**, 12.6 μs for the **CD**, and 10.2 μs for the **CP**. This was an increase in lifetime relative to $[Ru(tpy)_2]^{2+}$ of 24% for the **CM** and 13% for the **CD** and a decrease in lifetime of 8% for the **CP**. If the compounds in the series are compared, there is a decrease of 10% in the lifetime when going from the **CM** to the **CD** and of 19% when going from the **CD** to the **CP**. The lifetimes of the rigid chiral series were found to decrease slightly from 11.6 μs for the **RCD** to 10.8 μs for the **RCP**. None of these numbers is statistically different from that of the model compound where the lifetime was 11.1 μs.

Luminescence Lifetimes at 298 K. As described in the Experimental Section, a TCSPC setup was used in conjunction with a femtosecond laser system to obtain room-temperature lifetimes of the all species. Normalized fluorescence decay profiles for the chiral series with the corresponding single-exponential fits indicated by a solid line are shown in Figure 4a, and the corresponding lifetimes are shown in Table 1. The lifetimes at RT were found to increase to some extent in the chiral series from 280 ps for the **CM** to 345 ps for the **CD** and 365 ps for the **CP**.

Decay profiles of the rigid chiral series are shown in Figure 4b, with the corresponding lifetimes shown in Table 1. The somewhat higher χ^2 value (1.60) for the **RCD** was a consequence of the 82 MHz repetition rate (12.2 ns between pulses) of the Ti:sapphire laser in relation to the fluorescence lifetime of 3.5 ns for the **RCD**. The lifetime was still within the range of the laser system, but a larger error (15%) was expected. The data for the **RCP** were best fit by a biexponential decay. Both a very short lifetime of 50 ps was extracted as well as a much longer lifetime of 1.1 ns.

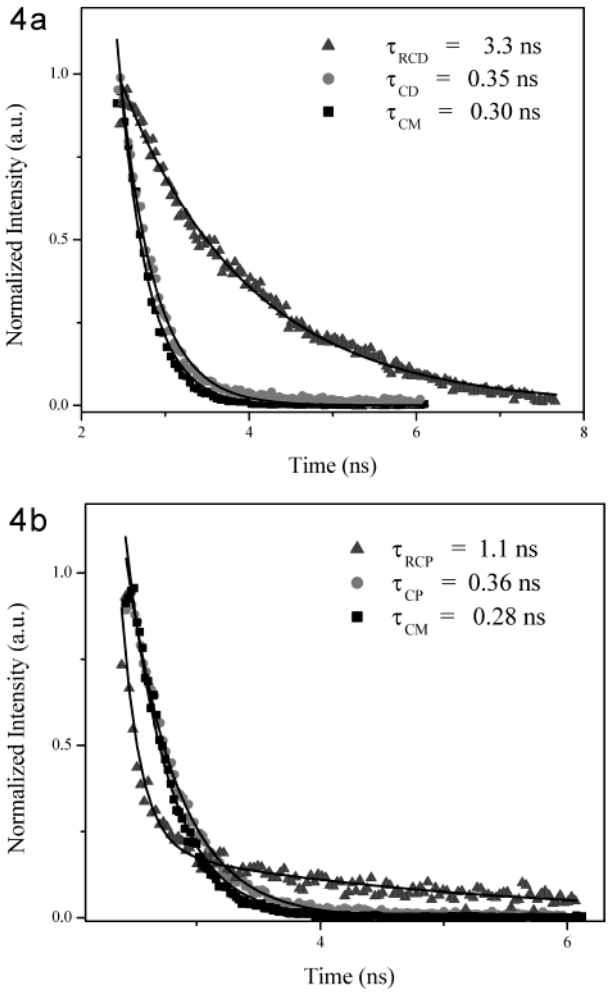

Figure 4. Emission decay profiles at 298 K in butyronitrile of (a) **CM**, **CD**, and **RCD** and (b) **CM**, **CP**, and **RCP**. The solid line represents the best fit of the data to a single-exponential decay.

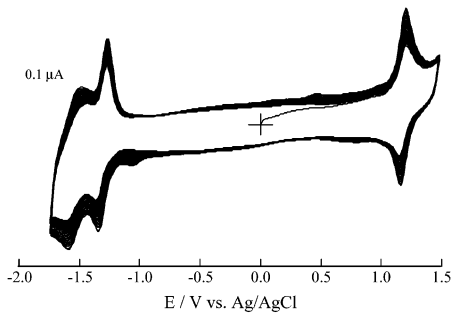

Figure 5. Consecutive cyclic voltammograms for a Pt electrode in contact with a 0.10 M TBAH/AN solution containing 0.1 mM (monomer unit) of ((−)-[ctpy-x-ctpy]-{Ru((−)-[ctpy-x-ctpy])}$(PF_6)_2$}$_n$. The scan rate is 100 mV s^{-1}.

Electrochemistry. Figure 5 shows a typical cyclic voltammogram for a 0.10 M TBAH/AN solution containing 0.1 mM (monomer unit) of the CP. The waves centered at +1.18 V vs Ag/AgCl correspond to a metal-localized Ru(II/III) redox reaction and are typical of bis(terpyridyl) coordination around a Ru center. In the negative potential range, two redox waves centered at −1.32 and −1.54 V, corresponding to ligand-based redox reactions, were observed. The increase in current with continuous potential scanning indicates the accumulation of an electroactive film on the electrode

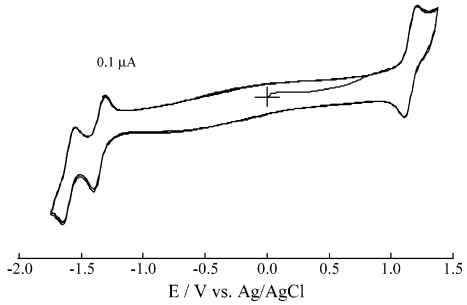

Figure 6. Consecutive cyclic voltammograms for a Pt electrode in contact with a 0.10 M TBAH/AN solution containing 0.1 mM $[Ru((-)\text{-ctpy})_2](PF_6)_2$. The scan rate is 100 mV s^{-1}.

surface. The fact that the peak potential separation of all waves decreased upon successive potential scanning is also consistent with the accumulation of a film. Deposition of the polymer is further supported by EQCM studies (not shown) in which the frequency decreased during ligand-based reductions and increased during the ligand-based oxidations but did not return to the original value. The electrodeposition may be due, at least in part, to low solubility of the electrically neutral polymer, since it has a net zero charge after reduction of the two terpyridine ligands. Dissolution of the electrodeposited film would appear to be kinetically slow, thus leaving some part of film on the electrode surface. The frequency changes described above accompanying the redox reactions are consistent with the film acting in an anion exchange fashion, which indicates, as would be anticipated, that anions are the mobile species.

For the metal-centered redox process there was no increase in coverage with continuous scanning over the potential range of 0.0 to +1.5 indicating that no film deposition takes place, contrary to the results mentioned above for the ligand-based reduction. However, EQCM studies indicated the presence of an adsorbed film whose coverage was approximately one monolayer. The frequency changes associated with the metal-based oxidation (Ru^{II}/Ru^{III}) were, as above, consistent with anion exchange type behavior.

The chiral dimer (**CD**) (0.2 mM monomer unit) exhibited a cyclic voltammogram that was quite similar to that of the **CP** with waves centered at +1.17, −1.35, and −1.54 V vs Ag/AgCl in a 0.1 M TBAH/AN solution. The current also increased upon continuous potential scanning through the ligand-based reductions, indicating the accumulation of a film onto the electrode surface. However the overall increase in current (and thus, surface coverage) was smaller than that of the polymer. This is reasonable because the solubility for the dimer should be higher than that of the polymer. Again as in the previous case, no deposition was evident when scanning only over the metal-based oxidation peak. EQCM results were also consistent with anion exchange type behavior.

Figure 6 shows a typical cyclic voltammogram for a 0.10 M TBAH/AN solution containing 0.1 mM of the chiral Ru monomer (**CM**) with waves centered at +1.16, −1.36, and −1.60 V. These values are quite similar to those for $[Ru(tpy)_2]^{2+}$. The wave shape of both metal-based and ligand-based process are typical of diffusion-controlled systems. In

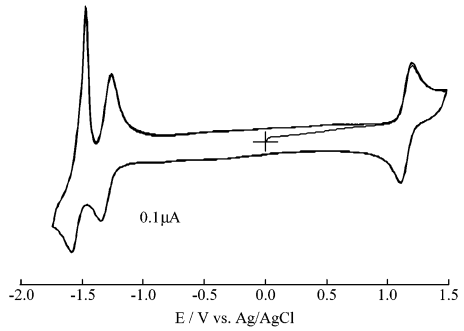

Figure 7. Consecutive cyclic voltammograms for a Pt electrode in contact with a 0.10 M TBAH/AN solution containing rigid chiral Ru dimer (0.1 mM of monomer unit). The scan rate is 100 mV s^{-1}.

addition, the current remained constant upon successive potential scanning. These results indicate that the chiral Ru monomer does not deposit upon potential scanning, likely due to its higher solubility in AN solution, even when it has a net zero charge after reduction of the ligands.

The cyclic voltammetric response of the rigid chiral Ru polymer (**RCP**) (0.1 mM of monomer unit) was qualitatively similar to that of the **CP** with waves centered at +1.15, −1.24, and −1.49 V. This material also appeared to deposit onto the electrode surface upon continuous potential scanning. EQCM studies revealed that the deposition takes place during the ligand-based reduction and that the deposited polymer effectively remained on the electrode surface upon reoxidation of the ligands.

The rigid chiral dimmer (**RCD)** (0.1 mM of monomer unit) exhibited a cyclic voltammogram similar to that of the chiral Ru dimer with waves centered at +1.15, −1.30, and −1.52 V (Figure 7). Whereas the Ru-centered redox wave appeared to be diffusional in shape, the wave shape of the ligand-centered reduction processes showed contributions from freely diffusing and surface-immobilized redox species. This was especially noticeable in the reoxidation waves where the processes appeared to be surface wave and/or stripping in shape. Upon successive potential scans, the cyclic voltammogram remained virtually constant, indicating that there is no continuous redox-active film deposition. This result was also supported by EQCM studies, which showed no overall decrease in the frequency upon continuous-potential scanning, although the frequency decreased during ligand-based reductions and increased during their subsequent oxidation.

In these types of transition metal complexes it is often found that the emission energy scales with the difference in formal potential for the metal-based oxidation and the first ligand-based reduction. Such correlation reflects the close coupling of the spectroscopic and electrochemical behavior of such materials. In the present case, we also observe a very good correlation ($R^2 = 0.96$) (Figure 8) between the emission energy and $\Delta E°$, indicating that, in this case as well, the processes are closely coupled.

A more detailed investigation of the electrochemical behavior of this and related redox polymers including admittance measurements of the quartz crystal resonator and studies of transport properties will be presented elsewhere.[22]

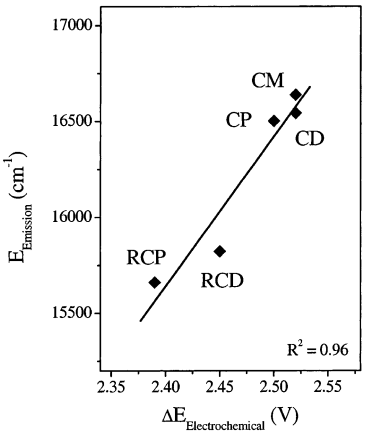

Figure 8. Plot of emission energy versus difference in formal potentials between the metal-localized oxidation and the first ligand-based reduction.

Discussion

The effects of spacers between chromophores in supramolecular systems are well documented.[13−16] One of the challenges in designing a spacer is to develop a system with extensive delocalization, typically using phenyl rings[17,18] or alkynes.[19] However, while lengthening the spacer can enhance delocalization, rigidity can be lost. In a rigid complex, the lowest energy geometry has a higher probability of being maintained than in a system in which the molecule can move freely, thus sampling many different geometrical arrangements, each with a unique energy. For example, in a bimetallic complex, electronic communication is only possible when certain geometrical constraints are satisfied. If the metal centers are able to rotate freely, the probability of electronic communication is considerably diminished and the photophysical properties of the bimetallic complex would be expected to be similar to those of the reference compound with a single metal center. However, if the bimetallic complex is both rigid or trapped in a rigid matrix and exhibits electron delocalization, then the absorption and emission energies would be expected to decrease in a way that is qualitatively similar to a particle-in-a-box.

The effects of electron delocalization and rigidity are evident in the two series of chiral molecules discussed in this work at 298 and 77 K. At 298 K, the fluorescence lifetimes of the **CD** and **CP** were identical to each other and were about 25% longer than for the chiral monomer. However, when ligand **X** was replaced with ligand **B**, the luminescence lifetime was dramatically affected, by 1 order of magnitude, in the case of the **RCD**. It is somewhat difficult

(13) Balazani, V.; Juris, A.; Venturi, M.; Campagna, S.; Serroni, S. *Chem. Rev.* **1996**, *96*, 759−833.
(14) Hush, H. S. *Coord. Chem. Rev.* **1985**, *64*, 135−157.
(15) Reimers, J. R.; Hush, N. S. *J. Phys. Chem. A* **1999**, *103*, 3066−3072.
(16) Creutz, C.; Newton, M. D.; Sutin, N. *J. Photochem. Photobiol., A* **1994**, *82*, 47−59.
(17) Barigelletti, F.; Flamigni, L.; Balazani, V.; Collin, J.-P.; Sauvage, J.-P.; Sour, A.; Constable, E. C.; Cargill Thompson, A. M. *J. Am. Chem. Soc.* **1994**, *116*, 7692−7699.
(18) Collin, J.-P.; Laine, P.; Launay, J.-P.; Sauvage, J.-P.; Sour, A. *J. Chem. Soc., Chem. Commun.* **1993**, 434−435.
(19) Grosshenny, V.; Harriman, A.; Ziessel, R. *Angew. Chem., Int. Ed. Engl.* **1995**, *34*, 1100−1102.

to compare the **RCD** and the **RCP** because of the biexponential nature of the decay of **RCP**. Lindsey et al. report energy transfer, with rates on the order of $(50\ ps)^{-1}$, between nonadjacent porphyrin centers in diphenylethyne-linked porphyrin trimers containing Mg, Zn, and free-base porphyrins.[20] The two mechanisms proposed were a superexchange or a hopping mechanism, which could also explain the very short lifetime (50 ps) measured for the **RCP**, though we have no direct experimental evidence of this. A double exponential decay could also arise as a result of heterogeneity within the polymer, but again, we have no evidence to support such an assertion. If the very short lifetime can be disregarded as an impurity, though we have no direct evidence of this, then we would just consider the second lifetime (1.1 ns), which is similar to that of the **RCD** (3 ns). No conclusions about the effects of polymerization on the emission energy were available because of the low emission yield. However, the absorption spectra at 298 K show dramatic red shifts in the MLCT emission maxima of the **RCD** (492 nm) and the **RCP** (503 nm) complexes when compared to the complexes based on ligand **X** that are all centered around 475 nm. If only chain length were considered, one would expect that a decrease in emission energy for the **RCP** would stabilize the excited state in tandem with an increase in the lifetime as the length of the polymer increased, analogous to a particle-in-a-box. Instead, the lifetime of the **RCD** is approximately three times longer than the long-lived component of the **RCP**. One explanation for the observed lifetime, which is in fact shorter compared to the **RCD**, is that favorable geometrical configurations become less probable as the number of Ru centers increases, leading to shorter lifetimes. For example, in the simpler case of a trimetallic complex, the two outside metal centers must simultaneously achieve the appropriate arrangement with the metal center in the middle as opposed to a dimer in which only two Ru center must simultaneously achieve a favorable arrangement.

Further evidence that geometric arrangements play a role in determining the luminescence lifetimes of these multimetallic complexes are the results obtained at 77 K. Confining the molecules in a rigid glass matrix resulted in nearly identical lifetimes for both series of polymers. The **CM** exhibits the longest lifetime (14 μs) followed closely by the **CD**, **CP**, **RCD**, and **RCP** ($12.6 \geq \tau \geq 10.8\ \mu s$). The small differences can be rationalized by assuming that it is more difficult to achieve the lowest energy configuration in the case of the **CD**, **RCD**, **CP**, and **RCP** as their sizes increase.

Table 2. Radiative and Nonradiative Decay Rates for the Series of Chiral Complexes

	$10^{-4}k_{nr}$ (s^{-1}) 77 K	$10^{-4}k_{r}$ (s^{-1}) 77 K	$10^{-9}k_{nr}$ (s^{-1}) 298 K	$10^{-2}k_{r}$ (s^{-1}) 298 K
$[Ru(tpy)_2]^{2+}$	4.70	4.31	8.00	80
CM	5.86	1.29	3.54	1.33
CD	7.06	0.87	2.90	6.64
CP	8.53	1.27	2.74	7.42
RCD	7.94	0.69	3.00	0.5
RCP	8.16	0.83	8.80	1.65

It is well established that geometric strain makes the energetically close ^{3}MC state more accessible in the case of $[Ru(tpy)_2]^{2+}$ when compared to $[Ru(bpy)_3]^{2+}$, which is a relatively unstrained bidentate ligand. This difference in strain is responsible for the observed picosecond lifetime and very low quantum yield of $[Ru(tpy)_2]^{2+}$ since relaxation from the ^{3}MC state is via nonradiative decay. At low temperatures, there is not significant thermal energy to populate the ^{3}MC state and, consequently, radiative processes govern the observed luminescence lifetime.[21] The results at low temperature provide a clear illustration of such behavior. The emission energy is considerably reduced in the case of the rigid spacer due to delocalization, decreasing by nearly 1000 cm^{-1}, but as discussed above, small differences in the lifetimes were observed. This indicates that the particle-in-the-box analogy adequately rationalizes the changes in emission energy but does not explain the changes in luminescence lifetimes, which are governed by the relative rates of radiative and nonradiative decay (Table 2).

Conclusions

The length of the delocalization "box" governs the absorption energy at 298 K and the emission energy at 77 K for the **RCD** and **RCP**. Dynamic changes in geometrical configuration at room-temperature establish the accessibility of the ^{3}MC state that dictates the observed luminescence lifetimes. The luminescence lifetimes at 77 K are not controlled by nonradiative decay, and consequently, similar lifetimes are observed. The small differences noted may be attributed to the larger barrier for the larger molecules to reach an energetically favorable arrangement.

Acknowledgment. This work was supported by the Cornell Center for Materials Research (CCMR), a Materials Research Science and Engineering Center of the National Science Foundation (Grant DMR-9632275). S.B. acknowledges a Fellowship for Advanced Researchers from the Swiss National Science Foundation (Grant 8220-053387).

IC020691V

(20) Lammi, R. K.; Ambroise, A.; Balasubramanian, T.; Wagner, R. W.; Bocian, D. F.; Holten, D.; Lindsey, J. S. *J. Am. Chem. Soc.* **2000**, *122*, 7579−7591.

(21) Kalyanasundaram, K. In *Photochemistry of Polypridine and Porphyrin Complexes*; Academic Press: San Diego, CA, 1992; pp 105−191.

(22) Takada, K.; Bernhard, S., Abruña, H. D. Manuscript in preparation.